

# Gentle Film Trapping Technique with Application to Drop Entry Measurements

Asen Hadjiiski,<sup>†</sup> Slavka Tcholakova,<sup>†</sup> Ivan B. Ivanov,<sup>\*,†</sup> Theodor D. Gurkov,<sup>†</sup> and Edward F. Leonard<sup>‡</sup>

Laboratory of Chemical Physics Engineering, Faculty of Chemistry, University of Sofia, 1164 Sofia, Bulgaria, and Department of Chemical Engineering, Columbia University, 520w 120th Street, New York, New York 10027

Received May 21, 2001. In Final Form: September 18, 2001

The film trapping technique, FTT, allows one to investigate the interactions between colloidal particles and a fluid interface that presses them against a flat solid substrate. The method was already applied for measuring the contact angles of micrometer sized latex spheres (Hadjiiski, A.; Dimova, R.; Denkov, N. D.; Ivanov, I. B.; Borwankar, R. *Langmuir* **1996**, *12*, 6665.), and the interaction of white blood cells with adsorption layers of antibodies (Patrick, S. M.; An, H.; Harris, M. B.; Ivanov, I. B.; Braunshtein, N. S.; Leonard, E. F. *Ann. Biomed. Eng.* **1997**, *25*, 1072. Ivanov, I. B.; Hadjiiski, A.; Denkov, N. D.; Gurkov, T. D.; Kralchevsky, P. A.; Koyasu, S. *Biophys. J.* **1998**, *75*, 545.). A new modification of the equipment is now proposed (FTT-gentle), which significantly increases the accessible range of capillary pressures exerted to particles, starting from a virtually zero value. This is particularly important for studying the highly deformable particles (e.g., biological cells) or the oil drops, which easily coalesce with the interface, like those used to promote a foam collapse (so-called antifoams). The basic principles of operation with FTT-gentle, illustrated with experiments and theoretical calculations of the shape of the interface around the trapped particle and the position of the three-phase contact line at the particle surface, are described. The feasibility of FTT-gentle is demonstrated by measuring the drop entry barriers (the critical capillary pressure inducing the coalescence of drops with the air–water interface) of several antifoams. The results show that the drop entry barrier strongly depends on the used surfactant and its concentration, and can be significantly decreased by addition of hydrophobized solid particles in the oil drops.

## 1. Introduction

In three recent papers<sup>1–3</sup> we proposed a new method, the film trapping technique (FTT), for studying the interaction between micrometer-sized particles (latex particles, oil drops or white blood cells) and a fluid interface. Briefly, the method consists of forming a meniscus in a capillary, containing the studied solution, sucking the liquid out of the meniscus thus compressing the particle between the surfaces of the thin film that is formed, and determining the shape of the interfaces from the observed interference pattern. In refs 1 and 2 the drops and the white blood cells (WBC) were trapped in a symmetric film with two fluid interfaces, whereas in refs 1 and 3 the solid particles and the WBC, respectively, were pressed against a solid substrate. The method has both advantages and shortcomings compared with other available techniques.<sup>4–6</sup> One of the main advantages of

the FTT, which distinguishes this method from the other techniques for studying thin liquid films, is the ability for independent variation of the capillary pressure and the film size in wide ranges.

In comparison with the micropipet technique,<sup>4</sup> it is impossible to realize interaction between two cells (identical or different), so that one of the surfaces must be nonbiological – air–water or oil–water. On the other hand, one can observe many cells (drops) simultaneously, which allows one to make statistics over the observations in a single experiment. The contact angle between the cell and the interface (which allows the calculation of the interaction energy and force: see ref 2) is measured interferometrically with higher precision than with the gonyometric method.

Another technique applicable for study of films between oil drops and liquid interface was described recently.<sup>5,6</sup> In this technique, the drop is supported on the tip of a micropipet and is pushed up with controllable force to a liquid interface. This method allows one to obtain isotherms of the disjoining pressure vs film thickness. However it is suitable only for investigation of single oil drops, whose size is restricted by the diameter of the micropipet used. The range of capillary pressures is also restricted. The method cannot be used for pressures below ca. 50 Pa.

In the last years a new modification of the micropipet technique was proposed<sup>7</sup> that allows one to study interaction between two drops manipulated by micropipets. This technique allows studying the ability of micron-sized emulsion drops to resist mutual coalescence or coagulation. Currently this method provides qualitative results only

\* To whom correspondence should be addressed. Laboratory of Chemical Physics Engineering, (formerly Laboratory of Thermodynamics & Physicochemical Hydrodynamics), Faculty of Chemistry, University of Sofia, 1 James Bourchier Avenue, 1164 Sofia, Bulgaria. Phone: (+359) 2 962 5310. Fax: (+359) 2 962 5643. E-mail: Ivan.Ivanov@LTPH.BOL.BG.

<sup>†</sup> University of Sofia.

<sup>‡</sup> Columbia University.

(1) Hadjiiski, A.; Dimova, R.; Denkov, N. D.; Ivanov, I. B.; Borwankar, R. *Langmuir* **1996**, *12*, 6665.

(2) Ivanov, I. B.; Hadjiiski, A.; Denkov, N. D.; Gurkov, T. D.; Kralchevsky, P. A.; Koyasu, S. *Biophys. J.* **1998**, *75*, 545.

(3) Patrick, S. M.; An, H.; Harris, M. B.; Ivanov, I. B.; Braunshtein, N. S.; Leonard, E. F. *Ann. Biomed. Eng.* **1997**, *25*, 1072.

(4) Evans, E. In *Physical Basis of Cell–Cell Adhesion*; Bondgrand, P., Ed.; CRC Press: Boca Raton, FL, 1988; p 173.

(5) Aveyard, R.; Binks, B. P.; Cho, W.-G.; Fisher, L. R.; Fletcher, P. D. I.; Klinkhammer, F. *Langmuir* **1996**, *12*, 6561.

(6) Binks, B. P.; Cho, W.-G.; Fletcher, P. D. I. *Langmuir* **1997**, *13*, 7180.

(7) Yeung, A.; Dabros, T.; Masliyah, J.; Czarnecki, J. *Colloids Surf.* **A 2000**, *174*, 169–181.

because it is difficult to obtain quantitative data about the emulsion films made by such kind of experiments.

In our previous studies<sup>1–3</sup> some problems were encountered with the control of the pressure exerted on the particles by the meniscus. The reason was that the compression of the particles was realized by suddenly withdrawing water through a side capillary, which led to fast thinning of the liquid layer, with eventual formation of a very thin equilibrium film. The resulting capillary pressure was high and the particle and meniscus interfaces were strongly deformed, which reduced the precision of the shape determination. With WBC,<sup>2,3</sup> the cells, whose membranes are at normal state ruffled (their surface is covered by numerous folds), were so strongly deformed that they unruffled. This casts doubt on the biological relevance of the results. Finally, once the film was formed, it was very difficult to decrease the capillary pressure, which made it virtually impossible to study the effect of variable force on the WBC behavior.

We propose now a modification of FTT, which we call *FTT-gentle*, in order to avoid the problem of strong deformation. The main differences are (i) The film can be formed by pushing out (rather than withdrawing) a fluid (air or liquid) from a capillary; (ii) By suitably adjusting the wettability of the capillary and the sharpness of its edge, one controls the shape of the meniscus in such a way that the meniscus capillary pressure, at the moment when the interface touches the particle, can be virtually zero, and can be varied smoothly back and forth during the experiment.

In the next section we describe the experimental apparatus. Section 3 is devoted to theoretical calculations of the shape of the interface around the particle and the position of the contact line as a function of the pressure exerted under different experimental conditions. The title of this section is “Principles of Operation”, because it is meant to provide the researchers information about what could be expected in experiments, depending on the properties of the system under study, and the way one can control their occurrence. In this section we present also several experimental results, which are compared with the theoretical predictions. As a demonstration of the new method, in Section 4, we have applied it for determination of the so-called “drop entry barrier” (critical capillary pressure to drop entry). This is a quantity, which characterizes the ability of small drops to pierce through the air–water interface.

## 2. Description of the New Film Trapping Apparatus

The apparatus is shown schematically in Figure 1. A vertical glass capillary tube 1 (of diameter of a few millimeters) is held a small distance apart from the flat bottom of a glass vessel 2. The lower capillary end is immersed in the liquid in the vessel. A positioning device (not shown) supports the capillary. This device allows *X*, *Y*, *Z* movement. An additional device allows adjustment of the capillary tilt so that the capillary tip can be set parallel to the substrate. The liquid in the vessel includes dispersed colloidal particles (e.g., emulsion droplets, solid particles, or biological cells). The particles could be also deposited on the substrate. The upper end of the capillary is connected by a three-way stopcock 3 to a gas-phase pressure control system consisting of two syringes 4, a precise pressure sensor 5, and a buffer volume as a pressure damping system 6. The two syringes, large and small, are for rough and precise pressure control, respectively. Micrometer screw 7 with spring 8 ensures precise

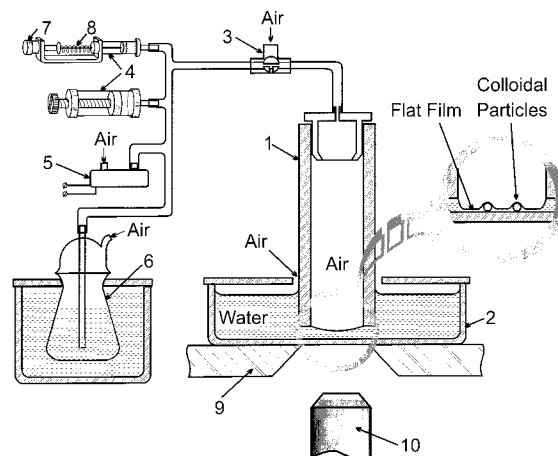


**Figure 1.** Film trapping apparatus. Basic scheme of the setup, allowing experiments with a freely moving air–water meniscus. A vertical glass capillary 1 is partially immersed in a vessel 2, containing water with dispersed colloidal particles. One can regulate the air pressure inside the capillary by means of a pressure control system in order to blow out the inner air–water meniscus. The gas-phase pressure control system consists of three-way stopcock 3, two syringes 4 (small and large), precise pressure sensor 5, and damping system 6, all connected with tubing. Micrometer screw 7 and spring 8 allow the precise pressure regulation by the smaller syringe. The capillary is supported by positioning device (not shown) mounted on a microscope stage 9. When the meniscus approaches the vessel's bottom at a distance smaller than the particle diameter, some particles remain sandwiched between the interface and the glass substrate (see the magnified part of the scheme). One observes the particles from below through the substrate by inverted microscope with objective 10.

motion of the piston of the small syringe. The damping system reduces pressure fluctuations arising from irregular movement of the syringe pistons and pressure drifts due to temperature gradients along the system tubing. This system consists of a thermostatically isolated flask, 6, containing water (see Figure 1), which is in contact with gas in the rest of the system through a vertical tube immersed in the flask. Besides stabilization of pressure, the damping system ensures saturation of the internal air phase with water vapor. This minimizes evaporation from the air–water interface shown magnified at the side of Figure 1. The positioning device with attached capillary and the vessel are mounted on the stage, 9, of an inverted microscope. The stage is equipped with the standard microscope *X*, *Y*, *Z* translators, and has an opening for observation from below through the glass bottom of the vessel by an objective 10 (Figure 1).

As mentioned in section 1, *FTT-gentle* allows one to trap particles at virtually zero capillary pressure, and consequently to precisely increase the pressure. This is achieved by making the interface flat before it touches the particles. (See also the explanations in section 3b.) One possible way to do this is to attach the interface at the edge of the capillary and to control its shape by changing the air pressure inside the capillary. The stable attachment of the air–water interface at the capillary edge, in the case of surfactant solutions, which improve the wettability of the capillary, is a difficult task. Small perturbations in the pressure or small mechanical vibrations in the system can provoke the detachment of the contact line from the edge. Then, the interface jumps from the edge and the contact line reaches a position at the internal wall of the capillary, corresponding to the equilibrium three-phase contact angle. One needs to use an edge with a special shape, made from poorly wettable

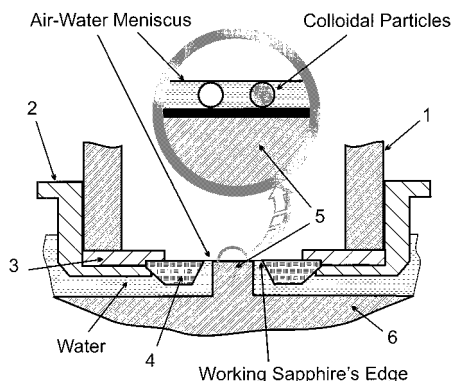


**Figure 2.** Modification of the film trapping apparatus, allowing experiments with an attached air–water meniscus (FTT-gentle setup). At the lower end of the glass capillary 1 a Teflon sleeve 2 is attached, that in combination with a Teflon washer 3, supports a sapphire disk 4 with a conical opening. The air–water meniscus is attached at the working sapphire's edge, situated at the upper side of the disk. A specially shaped glass substrate with a projecting upward stub 5 is used in experiments. The stub's base 6 is placed at the bottom of the vessel, shown in Figure 1. One can regulate precisely the air pressure inside the capillary in order to make the meniscus flat. This setup allows trapping the particles at virtually zero capillary pressure and then precisely to increase the pressure.

material, to ensure stable attachment of the fluid interface. A modification of the experimental setup, allowing experiments with an attached meniscus, is shown in Figure 2. The lower end of the capillary 1 is inserted hermetically in a Teflon sleeve, 2. The purpose of the sleeve, in combination with a Teflon washer 3, is to fasten a sapphire disk 4 to the capillary. The disk has an opening with a wedge-like shape. The conical opening's surface is inclined at angle approximately  $60^\circ$  to the horizontal (Figure 2). This shape of the wedge ensures stable attachment of the air–water interface at the sapphire's upper edge. Because of the strong hysteresis of the contact angle at the edge, the interface will detach only if one lowers significantly (much more than typical pressure fluctuations) the pressure inside the capillary.

However, since the sapphire disk is of finite thickness, it is impossible to move the attached air–water meniscus, keeping it flat, close to the glass substrate. This difficulty is overcome by elevating a part of the substrate surface with a small stub 5, cut out onto a glass plate 6. The plate lies on the vessel's bottom. The stub is projected upward into the opening of the sapphire. One can move the capillary downward in order to juxtapose the interface with the glass stub. Thus one achieves trapping of particles by a truly flat interface (see the magnified part of Figure 2).

One can maintain the attached meniscus flat by adjusting the air pressure inside the capillary. One can check whether the interface is really flat by several means. For example, observation in reflected light could be used to determine the interface shape (see, e.g., refs 1 and 2). One can observe tracer particles sliding below the curved water surface due to the action of buoyancy. The particles do not move when the interface is flat.

Before measurement, the tilt of the capillary must be regulated. One starts by adjusting the capillary so that it is visually vertical. There are several ways for precise adjustment. If one works with capillary without sapphire disk (a *freely moving meniscus*: see section 3c), one can use a simple method based on observing the appearance of bubbles. The capillary is lowered carefully until it touches the vessel's bottom. The air pressure is increased

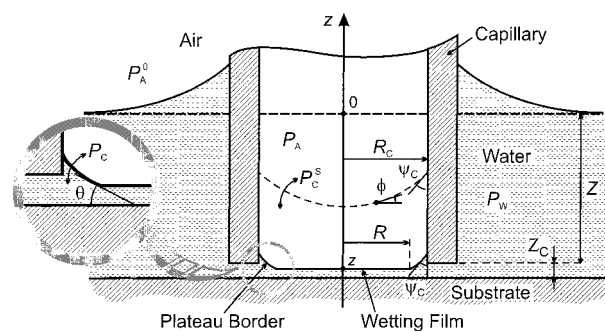


**Figure 3.** A scheme of water menisci formed around the capillary, with radius  $R_C$ . The outer meniscus decays to a flat interface away from the capillary. The lower capillary edge is held a small distance  $Z_C$  above the substrate and at a distance  $Z$  from the level of the flat surface of water in the vessel. The inner spherical meniscus (denoted with dashed line) with running slope angle  $\phi$ , and capillary pressure  $P_C^S$  has an equilibrium angle  $\psi_C$  with the capillary. This scheme corresponds to the case of a *freely moving meniscus*. When the interface moving downward, driven by the increasing pressure  $P_A$ , reaches the substrate, a wetting film with radius  $R$  forms. The wetting film is in equilibrium with the Plateau border whose capillary pressure is  $P_C$ . The equilibrium contact angle with the substrate is  $\theta$ .

until bubbles appear, escaping between the capillary tip and the vessel's bottom. The capillary is slightly lifted, the tilt is appropriately changed and this procedure is repeated until no more bubbles appear as the pressure is increased up to the maximal working value. The capillary is lifted again, the vessel is exchanged with that containing the studied dispersion of particles, the capillary is lowered to a suitable height, and the measurements are started. In the case of sapphire disk mounted at the end of capillary (an *attached meniscus*: see section 3b), it is recommended to perform tilt adjustment "on dry", by means of optical observation. One brings the lower sapphire surface into the focus of the microscope and adjusts the capillary tilt until the whole surface comes at the same focal plane. This method is slower but more precise and avoids accidental wetting of the sapphire's upper surface, which is unwanted because leads to easier detachment of the air–water interface.

### 3. Principles of Operation

Although some experimental observations will be presented in this section, full details about the materials used and the equipment are given in section 4.

If the manipulations are performed slowly enough, the shape of all interfaces in the system are governed by Laplace equation of capillarity<sup>8,9</sup> (see Figure 3 for notations):

$$\frac{1}{r} \frac{d}{dr}(r \sin \phi) = \frac{P_C}{\sigma} + \frac{\rho g z}{\sigma} \quad (1)$$

$$\frac{dz}{dr} = \pm \tan \phi = \pm \frac{\sin \phi}{\sqrt{1 - \sin^2 \phi}} \quad (2)$$

where  $\phi$  is the running slope angle,  $\sigma$  is the interfacial tension,  $\rho$  is the water density, and  $g$  is the acceleration of gravity. The capillary pressure is  $P_C = P_A - P_W$ , where

(8) Princen, H. M. In *Surface and Colloid Science*; Matijevic, E., Ed.; Wiley-Interscience: New York, 1969; Vol. 2, p 1.

(9) Kralchevsky, P. A.; Danov, K. D.; Denkov, N. D. In *Handbook of Surface and Colloid Chemistry*; Birdi, K. S., Ed.; CRC Press: New York, 1997; Chapter 11.

$P_A$  and  $P_W$  are the equilibrium pressures in the gas and liquid phases, respectively. To simplify the treatment we have neglected hereafter the term accounting for the gravity in the right-hand side of eq 1. Really, one can estimate<sup>1,2</sup> that in our case the term  $\rho g z$  is of the order of  $10^{-2}$  Pa while the  $P_C$  is typically above 1 Pa (or much higher, depending on the studied system).

When the microparticle is deformable, e.g., a WBC or a liquid drop, the analysis becomes rather complicated (see ref 2), but it is performed essentially in the same way as for nondeformable, solid particles. On the other hand, our goal here is only to demonstrate the main features of the processes involved. Hence, to make the analysis more transparent, we will deal only with nondeformable, spherical particles in the following three cases.

**(a) Freely Moving Meniscus, Forming a Wetting Film without Particles.** The analysis is commenced with a system without particles and assumes, that the meniscus can move freely inside the capillary, forming a contact angle  $\psi_C$  (see Figure 3) with the capillary wall. When the meniscus inside the capillary is away from the substrate (shown with dashed line in Figure 3), it has a spherical shape and its capillary pressure is

$$P_C^S = \frac{2\sigma}{R_C} \cos \psi_C \quad (3)$$

When the meniscus “touches” the substrate, a planar thin film forms suddenly. The film radius is  $R$  and the contact angle it forms with the meniscus, encircling it, is  $\theta$  (see the magnified part in Figure 3). The capillary pressure of this meniscus can be calculated by integrating once eq 1, with the boundary conditions  $\phi = \theta$  at  $r = R$ , and  $\phi = (\pi/2 - \psi_C)$  at  $r = R_C$ . The result is<sup>10,11</sup>

$$P_C = \frac{2\sigma(R_C \cos \psi_C - R \sin \theta)}{R_C^2 - R^2} \quad (4)$$

Equation 4 applies also in the absence of a wetting film: in this case  $\theta$  is the contact angle between the meniscus and the solid substrate and  $R$  is the radius of the “dry” spot. In Figure 4  $P_C$ , calculated from eq 4, is plotted vs  $R$  for two different contact angles,  $\theta_2 > \theta_1$ . Point A corresponds to a spherical meniscus. If the meniscus motion is extremely slow, the film forms with an initial radius  $R_{INI}$  and a contact angle  $\theta_1$  (point B). The new meniscus, encircling the film, has the same capillary pressure as the initial spherical meniscus. Even if one moves the spherical meniscus downward infinitely slowly, the initial film cannot have a radius smaller than  $R_{INI}$ . By setting  $P_C^S = P_C(\theta)$  and using eqs 3 and 4, one can derive

$$R_{INI} = R_C \frac{\sin \theta}{\cos \psi_C} \quad (5)$$

If one applies an air pressure higher than the equilibrium pressure  $P_A$ , corresponding to eq 3, one can form a film with a larger initial radius (point C). After the film has been formed, one can increase or decrease its radius by increasing or decreasing the gas pressure. Since the pressure in the liquid remains constant, this corresponds to an increase or decrease of the capillary pressure. Provided that there is no hysteresis of the contact angle, these pressure changes will correspond to a motion along

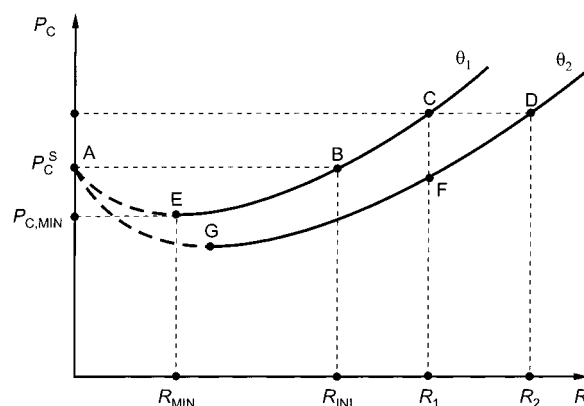


**Figure 4.** Plot of the capillary pressure  $P_C$  as a function of the film radius  $R$  for two different contact angles with the substrate  $\theta_2 > \theta_1$  at a constant contact angle with the capillary  $\psi_C$ , (see eq 4). Point A corresponds to a spherical meniscus with capillary pressure  $P_C^S$  given by eq 3. The film forms with initial radius  $R_{INI}$  at the same capillary pressure as that of the spherical meniscus (dashed line A–B). If one applies a pressure higher than the equilibrium pressure, one can form a film with a larger initial radius  $R_1$  (point C). After the film has been formed, one can increase or decrease the film radius along the path E–B–C by increasing or decreasing the pressure. For  $R < R_{MIN}$  the film is unstable and jumps to a spherical meniscus (point A). A possible transition from common black film to Newton black film is depicted with dashed line C–D. The transition is associated with an increase of the contact angle with the substrate to the value  $\theta_2$ . This process takes place at a constant capillary pressure and the final equilibrium state is reached at a new, larger radius  $R_2$ . In case of hysteresis, if one tries to close the film formed at point C, the film radius at the beginning will stay constant. If  $\theta_2$  is the value of the advancing contact angle, the instantaneous contact angle will increase (and the capillary pressure will decrease along the line C–F) until the curve corresponding to  $\theta_2$  is reached. After that the film will start shrinking along the curve F–G.

the curve B–C (and farther toward the higher radii) or along the curve B–E down to point E, where the film radius is  $R_{MIN}$ . However, it is impossible to obtain a film with radius smaller than  $R_{MIN}$ . The dashed portion of the curve corresponds to an unstable meniscus. At point E (corresponding to  $dP_C/dR = 0$ ) the film will close spontaneously and the system will suddenly jump to a spherical meniscus (point A). It is easy to obtain  $R_{MIN}$  and the corresponding capillary pressure  $P_{C,MIN}$  from eq 4:

$$R_{MIN} = R_C \frac{(\cos \psi_C - \sqrt{\cos^2 \psi_C - \sin^2 \theta})}{\sin \theta} \quad (6)$$

$$P_{C,MIN} = \frac{2\sigma \cos \psi_C - a \sin \theta}{R_C (1 - a^2)}, \quad a = \frac{R_{MIN}}{R_C} \quad (7)$$

The respective expressions for a perfectly wetting meniscus ( $\psi_C = 0$ ) are

$$R_{MIN} = R_C \tan \frac{\theta}{2} \quad (8)$$

$$P_{C,MIN} = \frac{2\sigma}{R_C} \cos^2 \frac{\theta}{2} \quad (9)$$

In practice the minimum is so shallow, that for purely technical reasons it is usually impossible to reach  $R_{MIN}$ . The pressure difference  $P_C^S - P_{C,MIN}$  (i.e., the depth of the minimum) can be expressed for  $\psi_C = 0$  as follows:

(10) Exerova, D.; Ivanov, I. B.; Scheludko, A. In *Research in Surface Forces*; Derjaguin, B. V., Ed.; National Bureau of Standards: Washington, DC, 1964; p 144.

(11) Toshev, B. V.; Ivanov, I. B. *Colloid Polym. Sci.* **1975**, *253*, 558.

$$P_C^S - P_{C,\text{MIN}} = \frac{2\sigma}{R_C} \sin^2 \frac{\theta}{2} \quad (10)$$

It is so small that any attempt to decrease the film radius below  $R_{\text{INI}}$  would lead to closure of the film.<sup>12</sup> Indeed, for reasonable values of the system parameters ( $\sigma = 35$  mN/m,  $R_C = 0.2$  cm,  $\theta = 1^\circ$ , and  $\psi_C = 0^\circ$ ), the difference  $P_C^S - P_{C,\text{MIN}}$  is of the order of  $10^{-2}$  Pa. Therefore, in the presence of a wetting film, it is impossible to reach capillary pressures lower than that of a spherical meniscus. It follows from eqs 3 and 4 that one practical way to decrease the meniscus capillary pressure is to increase the contact angle  $\psi_C$  between the meniscus and the capillary. This option is discussed below.

Finally, one may anticipate a transition from a common black film (CBF) to a Newton black film (NBF), depicted with dashed line  $C-D$ . The transition is associated with an increase of the contact angle with the substrate from  $\theta_1$  to a value  $\theta_2$ . This process takes place at constant capillary pressure, and the final equilibrium state is reached at a new, larger radius  $R_2$ . This explains the spontaneous expansion of a film, when it is transformed from CBF to NBF.

**(b) A Particle Trapped by a Meniscus Attached at the Capillary Edge.** If the edge of the capillary is either very sharp or has a special shape, it is possible (by controlling the gas pressure) to adjust the meniscus to be perfectly flat (zero capillary pressure) when it is not in contact with the particles. (See also section 2.) Then, by means of the positioning device, the capillary can be moved downward until the distance between the capillary's edge and the substrate  $Z_C$  becomes equal to the particle diameter  $2R_P$ . As a result, the meniscus "touches" the particle. If the particle is attached firmly to the substrate, the contact line will expand swiftly and move downward until it reaches a position, at which the contact angle between the particle and the air–water interface acquires its equilibrium value  $\psi_P$  (the dashed line 1 in Figure 5 shows the shape of the meniscus at this moment).<sup>13</sup>

The position of the contact line at the particle, specified by the azimuthal angle  $\beta$ , at a given angle  $\psi_P$  (Figure 5) can be determined by solving the Laplace equation. From eqs 1 and 2, assuming negligible gravity and setting  $P_C = 0$ , with boundary conditions at the particle surface, the following equations result:

$$r = R_{\text{CONT}} = R_P \sin \beta \quad (11)$$

$$z = Z_{\text{CONT}} = R_P(1 + \cos \beta) \quad (12)$$

$$\phi = \psi_{\text{CONT}} = \psi_P - \beta \quad (13)$$

(12) Although we will not treat here the role of the hysteresis of the contact angle, it is worthwhile noting how the processes will occur if there is a hysteresis. With reference to Figure 4, let us assume that  $\theta_2$  is the advancing contact angle. If we try to close the film, formed at point  $C$  (by sucking in the air from the capillary), the film radius at the beginning will stay constant, the contact angle will increase and the capillary pressure will decrease along the line  $C-F$  until the curve corresponding to  $\theta_2$  is reached. After this moment the film will start shrinking along the curve  $F-G$ .

(13) Since at this moment the interfacial tension force at the particle contact line is directed upwards, as shown in Figure 5, the meniscus will exert on the particle an upward capillary force  $2\pi R_{\text{CONT}} \sigma \sin \psi_{\text{CONT}}$ . That is why, if the particle (presumed weightless) is not firmly attached to the substrate, the meniscus will detach it. At that the meniscus will become again horizontal with the particle attached at the interface in a position, ensuring that its contact angle with the air–water interface is  $\psi_P$ . Experimental observations confirm such behavior.

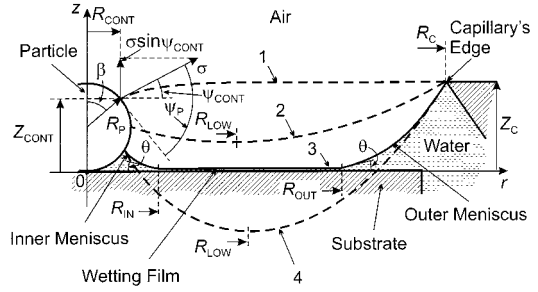


**Figure 5.** A particle trapped by an air–water meniscus that is attached at the capillary's edge, with radius  $R_C$ . The particle with radius  $R_P$ , and contact angle air–water–particle  $\psi_P$ , is placed at the axis of symmetry. The edge is situated at distance  $Z_C$ , from the substrate.  $\sigma$  is the interfacial tension.  $\beta$  is the azimuthal angle, which specifies the position of the contact line with radius  $R_{\text{CONT}}$ , height  $Z_{\text{CONT}}$ , and contact angle  $\psi_{\text{CONT}}$ . Curve 1 shows the meniscus shape at zero capillary pressure. Curve 2 corresponds to the case when  $P_C > 0$  before touching the substrate.  $R_{\text{LOW}}$  is the radius of the lowest interface point. With solid curve 3 the shape of the meniscus after "touching" the substrate is shown, when a wetting film constrained between radii  $R_{\text{IN}}$  and  $R_{\text{OUT}}$  is formed. The contact angle of the wetting film is  $\theta$ . Curve 4 corresponds to a hypothetical case without substrate, when meniscus freely bends downward with increasing  $P_C$ .

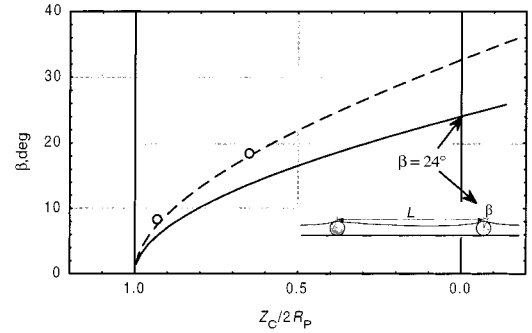


**Figure 6.** Plot of the azimuthal angle  $\beta$ , specifying the position of the contact line at the particle surface, calculated as a function of the relative vertical position ( $Z_C/2R_P$ ) of the edge for  $P_C = 0$ . The dashed curve corresponds to the case of a single particle. The points present experimental results, obtained for a single, hydrophilic glass bead ( $2R_P = 100 \mu\text{m}$ ). The case of two particles, separated at a distance  $L = 20R_P$ , is denoted with solid curve. The upper limit of  $\beta$ , obtained in experiments with many simultaneously studied glass beads, is  $10^\circ$ . Parameters used in the calculations are  $R_C = 0.2$  cm,  $R_P = 0.0025 R_C$ ,  $\sigma = 35$  mN/m,  $\psi_P = 0$ , and  $\theta = 0$ .

and one obtains

$$z(r) = c \ln(r + \sqrt{r^2 - c^2}) + Z_0 \quad (14)$$

$$c = R_{\text{CONT}} \sin \psi_{\text{CONT}} \quad (15)$$

$$Z_0 = Z_{\text{CONT}} - c \ln(R_{\text{CONT}} + \sqrt{R_{\text{CONT}}^2 - c^2}) \quad (16)$$

One can use eqs 11–16 to find the angle  $\beta$  (showing the position of the particle contact line) for a given position of the capillary edge, i.e., for

$$z = Z_C \text{ at } r = R_C \quad (17)$$

The azimuthal angle  $\beta$  calculated from eqs 14–16, as a function of the dimensionless  $z$ -position of the capillary's edge ( $Z_C/2R_P$ ) for  $P_C = 0$ , is shown in Figure 6. A value  $\psi_P = 0^\circ$  was chosen for this and the next calculations, since

such value is close to the real contact angle in the case of hydrophilic glass beads and oil drops. The dashed curve (corresponding to the case of single particle) at  $Z_C = 0$  (i.e., when the edge is at the level of the substrate) crosses the vertical line at angle  $\beta = 33^\circ$ . Hence, it is not possible to obtain larger values of  $\beta$ . Our experimental points for a single, hydrophilic glass bead, shown in the figure, are close to the theoretical prediction. These and the next experiments, mentioned in the current section, were performed with hydrophilic glass beads (Sigma) with diameter around  $100\ \mu\text{m}$  in aqueous solution of the anionic surfactant AOT (Sigma, catalogue no. D-0885) of 10 mM concentration.

The experiments with many glass beads, simultaneously trapped in the film, showed that the azimuthal angle does not exceed  $10^\circ$ . This is due to overlapping of the menisci around neighboring particles. To show that we used the theory from ref 14 and performed calculations of the interface for two particles at a distance  $L = 20R_p$ . The calculated solid line in Figure 6, corresponding to this case, shows that the maximum azimuthal angle is significantly lower ( $24^\circ$ ) than the angle calculated for a single particle. The value of the maximum azimuthal angle depends on the interparticle distance: the lower the distance, the lower the maximum angle  $\beta$  that can be achieved.

When the particles are very small, it is difficult to increase the radius of the contact line by smooth lowering of the capillary level. An alternative approach to achieve this is to start increasing the capillary pressure (by increasing the air pressure inside the capillary) after having established contact of the interface with the particle. A numerical simulation of this process is shown in Figure 7A ( $R_p = 5\ \mu\text{m}$ ,  $R_C = 0.2\ \text{cm}$ ,  $Z_C = 1.98 R_p$ ,  $\psi_P = 0$ ,  $\theta = 0$ , and  $\sigma = 35\ \text{mN/m}$ ). This figure shows the dependence of  $\beta$  on the dimensionless capillary pressure,  $p$ :

$$p = \frac{P_C}{2\sigma} R_p \quad (18)$$

The particle–interface contact is established at  $p = 0$  (curve 1 in Figure 5) and then  $p$  is raised. The interface bends downward as shown by curve 2 in Figure 5 until eventually it “touches” the substrate. At this moment a wetting film forms over the substrate (see curve 3 in Figure 5). Now the interface splits into two different zones: an inner meniscus, lying between the particle and the wetting film and an outer meniscus between the wetting film and the capillary’s edge. Both exist at the same applied capillary pressure. The film is confined between two coaxial circumferences with radii  $R_{\text{IN}}$  and  $R_{\text{OUT}}$  (see Figure 5). The numerical calculations reveal that at the beginning, before the film formation, the contact line expands very easily even with minor increase of the dimensionless capillary pressure. However, after formation of the wetting film, the dependence  $\beta(p)$  changes its behavior: the slope decreases and  $\beta$  tends to level off. The numerical results are shown with circles in Figure 7A. This behavior of  $\beta(p)$  is due to the fact that after formation of the wetting film, the boundary conditions for the inner and outer meniscus are different and lead to different solutions of Laplace equation. Before formation of a wetting film, the solution of Laplace equation is determined from the boundary conditions given by eqs 11–13 at the particle surface and

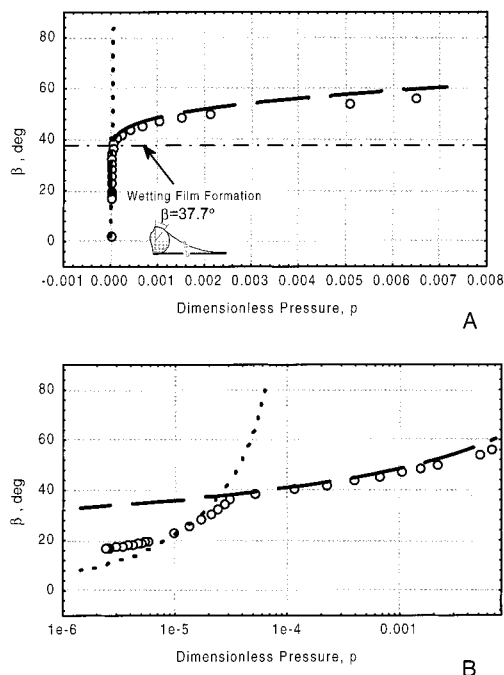


**Figure 7.**  $\beta$  as a function of the dimensionless capillary pressure  $p$  (defined in eq 18), plotted in a linear (A) and a logarithmic (B) scale. With circles the numerically obtained exact results are presented. With dotted line the asymptotic solution in the case without wetting film (see eq 19) is denoted. With long dashed line the asymptotic solution with wetting film (see eq 23) is denoted. The difference in the two functions is due to the change in the boundary conditions of the Laplace equation governing the shape of the menisci. Parameters used in the calculations are:  $R_C = 0.2\ \text{cm}$ ,  $R_p = 0.0025R_C$ ,  $\sigma = 35\ \text{mN/m}$ ,  $\psi_P = 0$ , and  $\theta = 0$ .

by eq 17 at the capillary’s edge. For illustration, one can express  $\beta(p)$  by the following asymptotic solution:

$$\beta(p) = \arccos \left( \frac{1 - \sqrt{(2 + \ln p)^2 + (1 + \ln p) \left( p \frac{R_C^2}{R_p^2} - 2 \frac{Z_C}{R_p} \right)}}{1 + \ln p} \right) \quad (19)$$

which is valid for

$$\psi_P = 0, \quad R_p \ll R_C \quad (20)$$

Two different menisci are formed after formation of the wetting film. The inner meniscus has boundary conditions at the particle surface given by eqs 11–13, and at the substrate:

$$\phi = -\theta, \quad z = 0 \quad \text{at} \quad r = R_{\text{IN}} \quad (21)$$

The outer meniscus has boundary conditions at the capillary’s edge given by eq 17, and at the substrate:

$$\phi = \theta, \quad z = 0 \quad \text{at} \quad r = R_{\text{OUT}} \quad (22)$$

Setting the contact angle with the substrate  $\theta = 0$  (complete wetting), one can express  $\beta(p)$  for the case with wetting film by the following asymptotic solution:

$$\beta(p) = \arccos \left( \frac{3 + \ln p}{1 + \ln p} \right) \quad (23)$$

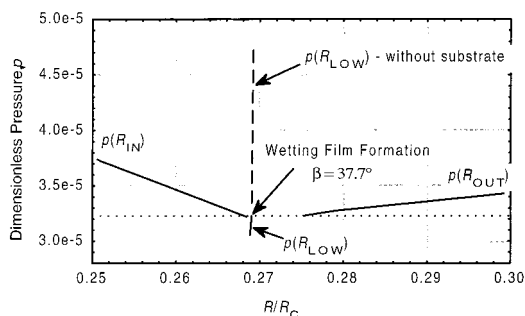


**Figure 8.** A diagram demonstrating the disproportion of the inner and outer menisci showed in Figure 5. It reveals the correlation between the dimensionless capillary pressure  $p$  (see eq 18), the radii  $R_{IN}$  and  $R_{OUT}$ , constraining the wetting film, and the radius  $R_{LOW}$  of the lowest point at the air–water interface. The solid line denoted with  $p(R_{LOW})$  correspond to the case prior to wetting film formation (curve 2 in Figure 5). The dashed line corresponds to the hypothetical absence of substrate, when the interface freely bends downward with increasing  $p$  (curve 4 in Figure 5). Parameters used in these calculations are  $R_C = 0.2$  cm,  $R_P = 0.0025R_C$ ,  $Z_C = 1.98R_P$ ,  $\sigma = 35$  mN/m,  $\psi_P = 0$ , and  $\theta = 0$ .

The plots of the two asymptotic solutions for  $\beta(p)$  are shown in Figure 7A: the case before formation of the wetting film (eq 19) with dotted line, and the case after wetting film formation (eq 23) with long-dashed line. The plot of the same dependencies in log scale, shown in Figure 7B, reveal a good agreement between the asymptotic solutions and the numerically calculated exact solution for  $\beta(p)$  around the point of wetting film formation. At this point, there is a sharp change in the slope (a kink) of the exact solution. One sees that in the first case the dimensionless pressure  $p$  appears in one nonlogarithmic term of eq 19, multiplied by a large number  $(R_C/R_P)^2$ , while in the second case  $p$  takes part only under logarithms. This explains the observed significant change in the  $\beta(p)$  behavior.

The wetting film expands asymmetrically with increasing  $p$ . A diagram demonstrating the relation between  $p$  and the two radii  $R_{IN}$  and  $R_{OUT}$  is shown in Figure 8 (see Figure 5 for notations). The almost vertical solid curve corresponds to the stage prior to the wetting film formation. A very small increase of the dimensionless capillary pressure to  $3.2 \times 10^{-5}$  is sufficient to provoke the formation of the wetting film. In practice, the wetting film forms immediately after beginning the increase of  $p$ . The dependence of the two film radii  $R_{IN}$  and  $R_{OUT}$  on  $p$  is different: the inner film radius  $R_{IN}$  decreases and changes less than the outer radius  $R_{OUT}$ , which increases. For comparison the radius  $R_{LOW}$  of the lowest point at the air–water interface is given also in the figure. The dashed line corresponds to the hypothetical absence of substrate (curve 4 in Figure 5) when the interface freely bends downward with increasing  $p$ . Our experiments confirmed the numerical predictions shown in Figure 8 for wetting film formation and its disproportionate expansion with increasing  $p$ .

We would like to summarize the main advantages of the experiments with a flat meniscus attached to the capillary edge. One of them is the possibility of trapping the colloidal particles at virtually zero capillary pressure and then increasing precisely the pressure. This possibility is very important for at least two kinds of experiments: those with highly deformable colloidal particles (biological cells or vesicles) and those with particles having a very low entry barrier (see section 4). Another advantage is that the problem with pushing the particles outward the

film, described in the following subsection, does not exist. This allows simultaneous trapping of many particles independently of their location with respect to the capillary's axis of symmetry.

**(c) A Particle Trapped by a Freely Moving Meniscus.** As mentioned earlier, it is difficult to experimentally realize the case allowing the best control of the capillary pressure: a meniscus attached at the capillary edge with zero capillary pressure. If the particles are only weakly deformable (and they also have not very low entry barrier), so that the initial capillary pressure need not be extremely low, one can use the method of *freely moving meniscus*, forming a contact angle  $\psi_C$  with the capillary. In this case it is also possible to realize relatively low initial capillary pressures if the contact angle  $\psi_C$  is about  $70^\circ$ – $90^\circ$  (see eqs 3 and 7). We will analyze this case by assuming that the particle on the substrate is located exactly at the axis of the capillary. This is not a very stringent limitation, because the slope of the meniscus around the axis of symmetry is very low (especially with high values of  $\psi_C$ ) and small shifts with respect to this position are immaterial. The originally spherical meniscus (with radius of curvature  $R_C/\cos \psi_C$ , which must be close to the capillary tip, is placed in contact with the particle either by extending it by means of the gas pressure or by lowering the position of the capillary. When contact is established, the contact line on the particle again expands until the equilibrium contact angle  $\psi_P$  is reached. The capillary pressure in this case is again given by eq 4, but the film radius  $R$  is replaced by the radius of the contact line  $R_{CONT}$  and the contact angle  $\theta$  by the angle  $\psi_{CONT} = \psi_P - \beta$  (see eqs 11–13). The position of the particle contact line is determined by Laplace equation. One can integrate eqs 1 and 2 using as boundary condition at the capillary wall:

$$r = R_C, \quad \phi = \frac{\pi}{2} - \psi_C \quad (24)$$

and eqs 11 and 12 at the particle surface. The result is

$$Z_C - Z_{CONT} = \pm \int_{R_{CONT}}^{R_C} \frac{\sin \phi}{\sqrt{1 - \sin^2 \phi}} dr, \\ \sin \phi(r) = \frac{1}{r} \left[ \frac{P_C}{2\sigma} (r^2 - R_C^2) + R_C \sin \psi_C \right] \quad (25)$$

In some particular cases, the integral can be solved analytically using elliptic integrals. Using eqs 11–13, 24, and 25, one can obtain the azimuthal angle  $\beta$  as a function of the capillary pressure  $P_C$ .

As described previously (subsection a: “Freely Moving Meniscus, Forming a Wetting Film without Particles.”), the minimal pressure exerted  $P_{C,MIN}$  (eq 7 or eq 9) is usually nonzero and depends on the contact angles.

Being simpler for experimental realization than the method with an *attached meniscus*, the method of particle trapping with a *freely moving meniscus* has some serious disadvantages. Achieving the contact angle with the capillary  $\psi_C$  close to  $90^\circ$  is a difficult task when the surfactant strongly increases the wettability of the capillary. Another disadvantage of this method in the case of an imperfectly hydrophobised capillary ( $\psi_C < 90^\circ$ ) is that the interface, moving downward, is convex and all particles which are not on the axis of symmetry are exposed to a radial force, which can carry them away from the film. This motion can completely prevent the particle trapping. Finally, when the freely moving meniscus comes close to the substrate, very often a lens shaped formation called

dimple<sup>15</sup> forms near the axis of symmetry. The thickness of the dimple is larger in the center and the wetting film forms at the periphery rather than in the center. The water inside the dimple is not in hydrostatic equilibrium with the surrounding water and the liquid drains out through the wetting film until the equilibrium is reached. Since the hydrodynamic resistance of the wetting film is significant, the process of dimple drainage may take a long time (minutes or hours). During this process, the observation of particles entrapped in the dimple is meaningless, because the capillary pressure is unknown.

#### 4. Experimental Section: Entry Barrier Measurements

In this section, as an illustration of the film trapping technique, we present some experimental results obtained with silicone oil-based emulsions. Our experiments are related to two different types of emulsions. The first one consists of pure oil droplets, and the second one of oil droplets containing small solid particles. The droplets of both types decrease foamability when dispersed in a foaming surfactant solution.

The actual mechanism of foam destruction by droplets of both types is still poorly understood. Many studies, however, confirm that the foam destruction includes a stage of formation and rupture of the asymmetrical air–water–oil film that appears when an oil drop approaches the foam film surface.<sup>16–20</sup> Therefore, the drop entry has a very important effect on foam stability of such systems.<sup>21–25</sup> Still there is a lack of quantitative measurements of the barrier that prevents the process of drop entry (i.e., the film rupture). Below we demonstrate the applicability of the FTT for measuring the critical capillary pressures to drop entry.

**Materials.** *Drop Entry Experiments with Surfactant–Booster Mixtures and Pure Silicone Oil Drops.* Mixtures of anionic alkylpolyoxyethylene sulfate (SDP3S) and amphoteric alkylamido-betaine (betaine), both provided by KAO Co., Japan, at four different molar ratios (in %): 100:0 (SDP3S alone), 80:20, 70:30, and 0:100 (betaine alone), with total concentration 0.1 M, were studied in our experiments. The ionic strength, due to the background electrolyte, was 66 mM for SDP3S (100:0) and 142 mM for betaine (0:100) solutions. The oil phase in all experiments was poly(dimethylsiloxane) (SH200, KAO Co., Japan).

*Drop Entry Experiments with Silicone Oil Drops Containing Solid Particles.* In these experiments we used a solution of the anionic surfactant dioctyl sulfosuccinate (AOT, Sigma, catalogue no. D-0885) with a concentration of 10 mM. Two emulsion formulations were studied. The first was pure poly(dimethylsiloxane) oil (Rhodia, France, 47V1000SH). The second contained hydrophobised silica particles (aggregates) of fractal structure, added in the same silicone oil. The silica aggregates had an average size in the micrometer range. In all experiments, deionized water from a Milli-Q system (Millipore, UK) was used for preparing the solutions.

(15) Ivanov, I. B.; Dimitrov, D. S. In *Thin Liquid Films*; Ivanov, I. B., Ed.; Marcel Dekker: New York, 1988; Chapter 7, p 379.

(16) Bergeron, V.; Cooper, P.; Fischer, C.; Giermanska-Kahn, J.; Langevin, D.; Pouchelon, A. *Colloids Surf., A* **1997**, *122*, 103.

(17) Exerowa, D.; Kruglyakov, P. M. *Foams and Foam Films*; Elsevier: Amsterdam, 1998; Chapter 9.

(18) Koczo, K.; Lobo, L. A.; Wasan, D. T. *J. Colloid Interface Sci.* **1992**, *150*, 492.

(19) Bergeron, V.; Fagan, M. E.; Radke, C. J. *Langmuir* **1993**, *9*, 1704.

(20) Koczo, K.; Koczona, J. K.; Wasan, D. T. *J. Colloid Interface Sci.* **1994**, *166*, 225.

(21) Basheva, E.; Ganchev, D.; Denkov, N. D.; Kasuga, K.; Satoh, N.; Tsujii, K. *Langmuir* **2000**, *16*, 1000.

(22) Hadjiiski, A.; Tcholakova, S.; Denkov, N. D.; Durbut, P.; Broze, G.; Mehreteab, A. *Langmuir* **2001**, *17*, 2426, 7011.

(23) Hadjiiski, A.; Denkov, N. D.; Tcholakova, S.; Ivanov, I. B. In *Proceedings of 13th International Symposium on Surfactants in Solution (University of Florida, Gainesville, June 11–16, 2000)*; Marcel Dekker: New York, 2001. In press.

(24) Denkov, N. D.; Marinova, K. *Proceedings of the 3rd EuroConference on Foams, Emulsions and Applications*; MIT: Bremen, 2000.

(25) Marinova, K.; Denkov, N. D. *Langmuir* 2001. In press.

**Table 1. The Type and the Main Parameters of the Used Pressure Sensors**

pressure transducer model (Omega Engineering, Inc., Stamford, CT)	pressure range, Pa	stated accuracy, <sup>a</sup> Pa	stated hysteresis and repeatability, Pa
PX274-01DI	±125	<±1.25	±0.31
PX163-005BD5V	±1 250	<±12.5	±3.1
PX142-001D5V	0–6900	<±51.8	±20.7

<sup>a</sup> Maximum deviation from the linear best fit for the whole pressure range.

**Methods.** Here some technical parameters of the experimental setup and the experimental procedures are given to complement the information from Sections 2 and 3. Glass capillaries with inner diameter  $2R_C$ , between 2 and 8 mm, were used. The capillary foreheads, held close to the substrate during the experiments, were optically polished. In the experiments with *attached meniscus* a polished sapphire monocrystal disk with a conical opening with angle  $60^\circ$  was mounted on the lower capillary's end by Teflon sleeve and washer (see Figure 2). The air–water interface was attached at the inner sapphire's edge, with a diameter of 4.4 mm, situated on the upper end of the disk. The height of the disk was 1.8 mm. The stub of the specially shaped glass substrate for experiments with an *attached meniscus* (see Figure 2) was 3 mm in diameter and was elevated 3 mm above its base. The stub's base consists of a circular plate with a diameter 30 mm and thickness 2 mm. The substrate was made from optical glass with polished plane parallel sides. The colloidal dispersion under study was poured into a glass Petri dish with a diameter of 60–80 mm. Its flat bottom was used as the substrate in experiments with a *freely moving meniscus* or for support of the specially shaped substrate in the case of *attached meniscus*. Prior to the experiments all parts, having contact with water, were washed with detergent, treated with mixture of potassium base, ethyl alcohol, and water, and amply rinsed with Millipore-MilliQ purified water. The capillary tubes, for experiments with a *freely moving meniscus*, were hydrophobized by drying in the oven at  $90–120^\circ\text{C}$  for 1–2 h in order to obtain a contact angle  $\psi_C$  typically about  $65^\circ–70^\circ$ . It should be noted that in contact with silicone oil spread over the water surface,  $\psi_C$  decreases to about  $45^\circ$ .

The pressure difference,  $\Delta P_A = P_A - P_A^0$ , between the pressure of the air in the capillary  $P_A$  and the pressure of the atmosphere  $P_A^0$ , was measured with a pressure sensor. The used pressure sensors are described in Table 1. The data acquisition equipment included a digital multimeter Metex M-4660A (Metex Instruments), connected to a PC.

The height of water in the vessel is  $Z + Z_C$ . ( $Z$  is the distance between the flat air–water interface and the lower capillary end and  $Z_C$  is the distance between the substrate and the capillary's end, see Figure 3). Thus the pressure at the bottom of the liquid is  $P_A^0 + \rho g(Z + Z_C)$ . If one neglects the small change of hydrostatic pressure inside the inner meniscus in the capillary ( $Z_C \ll Z$ ), one finds the following relationship between the capillary pressure  $P_C$  and the measured pressure difference  $\Delta P_A$ :

$$P_C = \Delta P_A - \rho g Z \quad (26)$$

$Z$  is measured during the capillary movement downward, from the reference position of contact with the water surface to the working position close to the substrate. A micrometer translator having accuracy of  $\pm 5 \mu\text{m}$  was used, providing a precision of  $\pm 0.05$  Pa for determination of the hydrostatic pressure (the last term in eq 26). The immersed volume of the capillary itself and the volume of water which flows inward to or outward from the capillary with the variation of  $P_A$ , have a relatively small influence on the referent water level in the vessel and therefore can be neglected.

The trapped oil drops were observed from below, through the substrate, with a Carl Zeiss Jena inverted microscope (objective Zeiss, LD Epiplan,  $20\times/0.40$ , with 9.8 mm working distance) in reflected monochromatic light ( $\lambda = 546$  nm) and in transmitted white light. The observation in reflected light provides an interference picture caused by the curved interfaces around the trapped particles.<sup>1,2</sup> The process of drop entry on the water

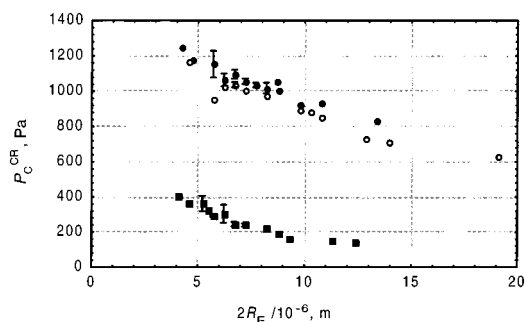


**Figure 9.** Critical capillary pressure to drop entry  $P_C^{CR}$  as a function of the equatorial drop diameter  $2R_E$  at different molar ratios of the surfactant-booster mixture SDP3S:betaine (70:30 is denoted with solid circles, 80:20 with empty circles, SDP3S alone with solid squares, the total surfactant concentration in all cases is 0.1 M). The experimental data for drops with similar size are represented as a mean value and a standard deviation (the error bar is not shown when it is smaller than the symbol size). In the case of betaine-alone solution, the critical capillary pressure exceeds the range of the pressure sensor ( $P_C^{CR} > 6900$  Pa). The experiments were performed with a *freely moving meniscus*.

surface, connected with changes of the drop shape, is clearly seen in both reflected and transmitted light. The observation in transmitted light allows measurements of the equatorial particle radii  $R_E$  with an accuracy of about  $\pm 0.8 \mu\text{m}$ . The equatorial radius  $R_E$  is involved in the case when the trapped particles are deformable. After deformation  $R_E$  becomes greater than  $R_P$ : the radius of the spherical particle. A digital CCD camera (Kappa CF 8/1 DX) and VCR (Samsung SV-4000W) was used to record the observed picture. All experiments were carried out at the ambient room temperature ( $T = 22 \pm 2^\circ\text{C}$ ). Water evaporation inside the capillary was avoided by performing the measurements under saturated water vapor.

The emulsion under study was prepared by adding  $50 \mu\text{L}$  of silicone oil (or mixture of silicone oil and solid particles) to 20 mL of surfactant solution. The emulsion was stirred for 1 h before the experiments, using a magnetic stirrer. A freshly stirred emulsion was poured into the Petri dish immediately before beginning each experimental run. We observed many (almost flat) oil lenses floating at the water surface. Along with the fact that the initial spreading coefficient of the oil is positive, this is an indication that the drop entry measurements were performed in the presence of a thin oil layer over the solution surface. The situation in real foams with oily additives is similar:<sup>26,27</sup> a portion of the oil rapidly spreads over the solution surface during foam formation.

During the experiment, one changes slightly the pressure in the capillary  $P_A$  so that the capillary pressure increases very slowly. After each small increment of pressure increase, one waits for several minutes to ensure a mechanical equilibrium, confirmed by the observation of the interference picture in reflected light. One observes that trapped drops enter the interface when a given, critical capillary pressure is reached. In some cases, the drops do not enter the interface at the applied pressures, because the entry barrier is higher than the accessible pressure range.

## 5. Results and Discussion.

**Drop Entry with Surfactant-Booster Mixtures and Pure Silicone Oil Drops.** The experiments were done with a *freely moving meniscus*, using PX163 and PX142 pressure sensors (see Table 1). The critical capillary pressure to drop entry  $P_C^{CR}$  as a function of the equatorial drop diameter  $2R_E$ , at three different surfactant molar ratios, is shown in Figure 9.  $P_C^{CR}$  is defined as the capillary pressure  $P_C$  measured at the moment of rupture of the

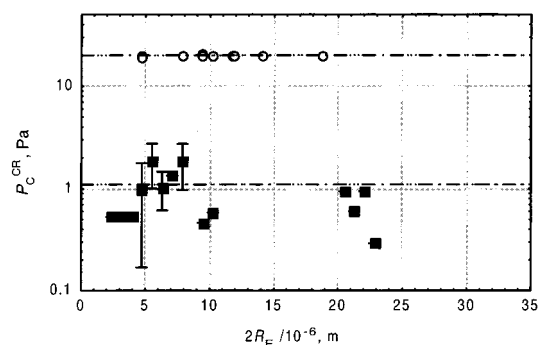


**Figure 10.** Critical capillary pressure to drop entry  $P_C^{CR}$  as a function of the equatorial drop diameter  $2R_E$  for emulsions based on pure silicone oil (empty circles) and mixture of silicone oil with solid particles (solid squares) in aqueous solutions of 10 mM AOT. The experimental data for drops with similar size are represented as a mean value and a standard deviation. The experiments were performed with an *attached meniscus*.

pseudoemulsion film between a drop and the air-water interface. Since many drops get simultaneously trapped, it was possible for each experimental run to record 1–10 drop entry events. The total number of drop entry events for each studied system exceeds 100. The experimental data for drops with similar size are represented as a mean value and an error bar for the standard deviation. When not shown, the error bar is smaller than the symbol size. One sees that in the case of SDP3S alone (solid squares in Figure 9) the values of the critical capillary pressure are smaller than 400 Pa. The addition of betaine to the mixture leads to a significant increase of the values of  $P_C^{CR}$ . In the case of an 80:20 mixture of SDP3S:betaine (empty circles in Figure 9) and at 70:30 molar ratio (solid circles),  $P_C^{CR}$  increases up to about 1200 Pa for the smallest drops. The experiments with betaine alone have shown that the critical capillary pressure is so large, that it exceeds the working range of the pressure sensor ( $> 6900$  Pa for PX142: see Table 1). This is not a limitation of the FTT but of the sensor used.

The tendency of the critical capillary pressure to increase with the molar fraction of betaine correlates with results from the foam stability tests.<sup>21</sup> The experiments described in ref 21 showed that the final height of stable foam in the testing cylinder increases with the molar fraction of betaine in the foaming solution. The increase of the height of the stable foam corresponds to increase of the critical capillary pressure. One can conclude that the foam boosting effect of betaine is directly related to the increase of the barrier to drop entry.<sup>21,23</sup> A trend for increase of the critical capillary pressure with diminishing the drop size is clearly seen in all three cases shown in Figure 9. This is probably connected with the augmented foam stability in the presence of smaller drops.<sup>21,23</sup>

**Drop Entry Experiments with Silicone Oil Drops Containing Solid Particles.** In these experiments we compared two different silicone oil emulsions, with and without solid particles, in solutions of the anionic surfactant dioctyl sulfosuccinate (AOT). The experiments were made with an *attached air-water meniscus*. These results were obtained with PX247 pressure sensor (see Table 1).

The critical capillary pressure to drop entry  $P_C^{CR}$  as a function of the equatorial drop diameter  $2R_E$  for both emulsions is shown in Figure 10. One sees that the barrier to drop entry for pseudoemulsion films stabilized with 10 mM AOT (Figure 10) is significantly lower than that for mixtures of SDP3S:betaine with 0.1 M total concentration

(26) Denkov, N. D.; Cooper, P.; Martin, J.-Y. *Langmuir* **1999**, *15*, 8514.

(27) Denkov, N. D. *Langmuir* **1999**, *15*, 8530.

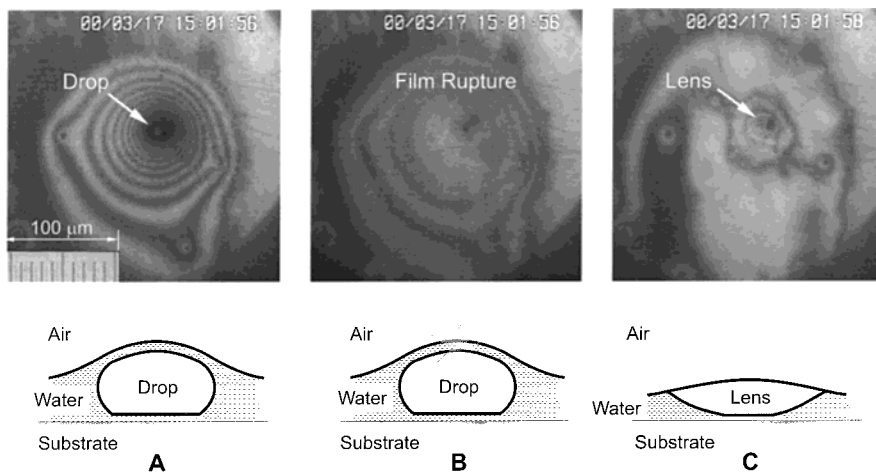


**Figure 11.** Microscope pictures from experiment with an *attached meniscus* that show consequent stages of the drop entry process. (A) The moment before drop entry. (B) The air–water–drop film is just ruptured. (C) An oil lens is formed. The capillary pressure for all pictures is about 1 Pa. The emulsion drops contain 4 wt % hydrophobic silica. The aqueous solution is 10 mM AOT.

(Figure 9). In the case of pure oil drops (empty circles in Figure 10) the mean  $P_C^{CR}$  is about 20 Pa; the addition of solid particles to the silicone oil (solid squares in Figure 10) leads to a strong decrease of  $P_C^{CR}$ : it becomes about 1.1 Pa. Microscope pictures in reflected light from these experiments, displaying the consequent stages of drop entry, are shown in Figure 11. The moment before drop entry is shown in A. The moment when the air–water–drop film is just ruptured is shown in B). After entry, the oil drop transforms to a lens (C). The capillary pressure is about 1 Pa for A–C. A reduction of the stability of asymmetric oil–water–air films by addition of hydrophobic solid particles was detected qualitatively in numerous previous studies.<sup>16,20,26–30</sup>

FTT-gentle provides an opportunity for obtaining a quantitative measure (the drop entry barrier  $P_C^{CR}$ ) that can be used for explanation of the antifoam activity. A correlation between the drop entry barrier and the antifoam activity was recently reported in a series of papers.<sup>21–25</sup>

**Disjoining Pressure in the Asymmetric Film Straddled between a Compressed Drop and Another Interface.** It is beyond the scope of this paper to attempt detailed interpretation of the mechanism of action of antifoam drops and particles. Nevertheless, it is pertinent to discuss briefly the relevance of the present measurements to the situation in real foams. It was shown<sup>23,26,27</sup> that, in a foam, the antifoam globules get trapped either in the foam lamellas (films) or in the Gibbs–Plateau borders. In either case they experience compression by the air–water interfaces, which is due to the capillary pressure in the Gibbs–Plateau borders (GPB). The latter pressure plays the same role as the applied capillary pressure in our FTT experiments, and one can argue that the bubble will burst when the capillary pressure of the GPB (or foam bubble) becomes equal to  $P_C^{CR}$ , measured by FTT. Since, however, the drop entry occurs through rupture of the asymmetric thin film, intervening between the drop and the bubble surface, it is important to connect the meniscus capillary pressure with the disjoining pressure in this film. This connection can be found by the following force balance.

Imagine, as depicted in Figure 12, that a drop is pressed by a curved interface (a bubble) with capillary pressure  $P_C^B$ , thus forming a small asymmetric film with the air–water interface. To make the treatment more transparent,

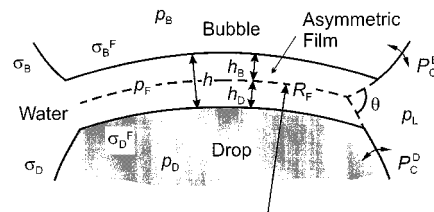


**Figure 12.** A drop is pressed by a curved interface with capillary pressure  $P_C^B$ , thus forming a small asymmetric film with the air–water interface. The surface of tension with radius of curvature  $R_F$  is situated between the film surfaces: at distance  $h_D$  from the drop and  $h_B$  from the bubble. The film has a total thickness  $h$  and a contact angle  $\theta$ .

we will assume that both surfaces of the film have the same radii of curvature  $R_F$  and that the interaction in the film does not affect significantly the surface tension of the air–water surface  $\sigma_B$  and the oil–water drop interfacial tension  $\sigma_D$  (the latter is true for not very large contact angles film–meniscus, say below  $10^\circ$ ). Let the pressures in the different phases be  $p_L$  in the liquid (water), containing the drop,  $p_B$  in the outer (bubble) phase,  $p_D$  inside the drop (oil), and  $p_F$  inside the film. Then

$$\frac{2(\sigma_B + \sigma_D)}{R_F} = p_D - p_B = (p_D - p_L) - (p_B - p_L) = P_C^D - P_C^B \quad (27)$$

where  $P_C^D$  and  $P_C^B$  are the capillary pressures at the drop and meniscus (bubble) interfaces, respectively. This equation allows calculating the film radius  $R_F$ :

$$\frac{1}{R_F} = \frac{P_C^D - P_C^B}{2(\sigma_B + \sigma_D)} \quad (28)$$

On the other side, the disjoining pressure  $\Pi$  in the film is defined as<sup>1,2</sup>

$$\Pi = p_F - p_L = (p_F - p_B) + (p_B - p_L) = \frac{2\sigma_B}{R_F} + P_C^B \quad (29)$$

By combining eqs 28 and 29 we reach the final result:

$$\Pi = \frac{\sigma_D}{\sigma_B + \sigma_D} P_C^B + \frac{\sigma_B}{\sigma_B + \sigma_D} P_C^D \quad (30)$$

The capillary pressure  $P_C$ , in the FTT experiments discussed above, in the present notation is actually  $P_C^B$ . Hence, it is possible to calculate from these equations and our data for  $P_C^{CR}$  the film radius and the critical disjoining pressure as well. Such calculations will be performed and discussed in a subsequent paper devoted to the role of entry barriers in antifoaming.<sup>22</sup> With  $P_C^B = 0$ , the above equations are valid for a drop attached to a planar fluid interface. We did not assume during the derivation anything about the drop shape, so that the results are valid also for a strongly deformed drop, but then its curvature must be either measured<sup>31</sup> directly or calculated by solving the Laplace equation (for details see refs 1 and 2).

If the “drop” is a solid spherical particle of radius  $R_p$ , one can formally substitute in eq 30  $P_C^D = 2\sigma_D/R_p$  and then set  $\sigma_D$  equal to infinity in the result:<sup>33</sup>

$$\Pi = \frac{\sigma_D}{\sigma_B + \sigma_D} P_C^B + \frac{\sigma_B}{\sigma_B + \sigma_D} \frac{2\sigma_D}{R_p} \approx P_C^B + \frac{2\sigma_B}{R_p} \quad (31)$$

The above derivation of the surface force balance, eq 30, was not entirely consistent, since we accounted for the disjoining pressure in the film, but neglected its influence on the two interfacial tensions. This was done to simplify the derivation and to make it physically more transparent. Although the role of the latter factor is often (but not always) negligible, we have accounted for it in the Appendix.

### Conclusions

The film trapping apparatus described here allows studying the interactions between colloidal particles and a liquid interface that presses them against a flat solid substrate. The experimental approach, termed FTT-gentle, is an extension of the recently proposed film trapping technique.<sup>1–3</sup> It is capable of determining the physicochemical parameters of thin films intervening between particles and a liquid interface. With FTT-gentle, a very wide range of capillary pressures can be exerted on entrapped particles whose size is typically between 1 and 50  $\mu\text{m}$ . The capillary pressure can be varied very precisely. More than one trapped particle can be observed simultaneously, which increases the productivity of the experiments. The feasibility of FTT-gentle is demonstrated by experiments for determination of the drop entry barrier with different silicone oil-based emulsions dispersed in foaming media. The drop entry barrier, which is of key importance for regulation of the foam stability, depends on the surfactant composition and can be significantly decreased by addition of solid particles in the oil drops.

(28) Garrett, R. P. In *Defoaming: Theory and Industrial Applications*; Marcel Dekker: New York, 1993; Chapter 1.

(29) Tamura, T.; Kageyama, M.; Kaneko, Y.; Kishino, T.; Nikado, M. *J. Colloid Interface Sci.* **1999**, *213*, 179.

(30) Wasan, D. T.; Christiano, S. P. In *Handbook of Surface and Colloid Chemistry*; Birdi, K. S., Ed.; CRC Press: Boca Raton FL, 1997; Chapter 6.

(31) In the case of large drops, it is actually easier to measure the film radius  $R_f$ , say by using differential interferometry,<sup>32</sup> and then calculate  $\Pi$  from eq 29.

(32) Nikolov, A. D.; Kralchevsky, P. A.; Ivanov, I. B. *J. Colloid Interface Sci.* **1986**, *112*, 122.

(33) An equation, similar to the expression after the last equality sign in eq 31 was recently derived in a different way by Bhatt et al.,<sup>34</sup> but instead of  $R_p$  in the denominator in the second term they have  $R_p + h$ , where  $h$  is the film thickness (see eq 4 in ref 34).

**Acknowledgment.** The fruitful discussions with Professor P. Kralchevsky, Professor N. Denkov, and Dr. K. Marinova are gratefully acknowledged. The authors are indebted to Miss M. Paraskova for drawing some of the figures.

### Appendix: Role of the Curvature and Interfacial Interactions on the Surface Force Balance

A more general form of eq 30 for the disjoining pressure of a film, straddled by two spherical interfaces<sup>35</sup> (see Figure 12), can be derived by using eqs 13, 26, and 33 in ref 36. Equation 13 is a force balance (similar to our eq 27), connecting the pressure drop across the film with the total film tension  $\gamma$  and the radius of curvature of the surface of tension  $R_F$ . Equation 26 in ref 36 connects the interfacial tensions  $\sigma_D^F$  and  $\sigma_B^F$  at the interfaces film-drop and film-bubble (the superscript F denotes that these quantities refer to the film) with the radii of the respective interfaces,  $R_D = R_F - h_D$  and  $R_B = R_F + h_B$ , and the disjoining pressure  $\Pi$ . Equation 33 in ref 36 establishes the connection between  $\gamma$  and all other quantities.

To make these equations simpler, we will take advantage of the facts that the ratios  $x_D = h_D/R_F$ ,  $x_B = h_B/R_F$ ,  $x = h/R_F$  (the film thickness is  $h = h_D + h_B$ ) are much smaller than unity and will expand these expressions in series with respect to the  $x$ 's by keeping only the linear terms. The results are (note that  $\Pi$  is of the order of the capillary pressures so that  $\Pi R_F$  is of the order of the interfacial tensions):

$$\frac{2\gamma}{R_F} = P_C^D - P_C^B \quad (A1)$$

$$\frac{2\sigma_D^F}{R_F}(1 + x_D) \approx P_C^D - \Pi(1 + 2x_D) \quad (A2)$$

$$\frac{2\sigma_B^F}{R_F}(1 - x_B) \approx -P_C^B + \Pi(1 - 2x_B) \quad (A3)$$

$$\gamma \approx \sigma_D^F(1 + x_D) + \sigma_B^F(1 - x_B) + \Pi R_F x \quad (A4)$$

For a planar film (infinite radius  $R_F$ ), they give the well-known relationships:<sup>36</sup>

$$P_C^D = P_C^B = \Pi; \gamma = \sigma_D^F + \sigma_B^F + \Pi h \quad (A5)$$

There are no problems in principle to solve the system of eqs A1–A4. However, this requires long and tedious calculations and the results are cumbersome and physically obscure, unless an explicit expression (valid for a specific system) for the dependence  $\Pi(h)$  is used. Such a solution is similar to accounting for the dependence of the surface tension  $\sigma$  of a drop on its radius  $R$ , leading to the well-known Tolman's equation:<sup>37,38</sup>  $\sigma(R) = \sigma_\infty(1 - 2\delta_\infty/R)$ , where  $\sigma_\infty$  is the surface tension of a planar interface (at infinite  $R$ ) and  $\delta_\infty$  is the distance between the equimolecular dividing surface and the surface of tension. Since  $\delta_\infty$  is usually smaller than 1 nm,<sup>39</sup> this correction to the

(34) Bhatt, D.; Newman, J.; Radke, C. J. *Langmuir* **2001**, *17*, 116.

(35) Since we neglected gravity effects, the film surfaces are spherical.

(36) Ivanov, I. B.; Kralchevsky, P. A. In *Thin Liquid Films: Fundamentals and Applications*; Ivanov, I. B., Ed.; Surfactant Science Series; Marcel Dekker: New York, 1988; Vol. 29, Chapter 2.

(37) Tolman, R. C. *J. Chem. Phys.* **1949**, *17*, 333.

(38) Kralchevsky, P. A.; Nagayama, K. *Particles at Liquid Interfaces and Membranes*; Elsevier: Amsterdam, 2001.

(39) Ono, S.; Kondo, S. *Molecular Theory of Surface Tension in Liquids*; Springer-Verlag: Berlin, 1960.

surface tension is significant only with extremely small drops and bubbles. In the present case, the film thickness (i.e.,  $h$ ,  $h_D$ , and  $h_B$ ) will play the role of  $\delta_\infty$  and the effect is expected to be somewhat larger (it may be important especially for microemulsion and/or micronsized drops), but the computation is worth the effort only if a specific system is considered.

That is why we will neglect all terms proportional to the  $x$ 's. Dividing eqs A2 and A3, after some rearrangement we obtain an equation analogous to eq 30, but now with the film interfacial tensions  $\sigma_D^F$  and  $\sigma_B^F$ , instead of the interfacial tensions between the respective *bulk* phases  $\sigma_D$  and  $\sigma_B$ :

$$\Pi = \frac{\sigma_D^F}{\sigma_B^F + \sigma_D^F} P_C^B + \frac{\sigma_B^F}{\sigma_B^F + \sigma_D^F} P_C^D \quad (\text{A6})$$

Although correct, this equation is not very convenient for experimental purposes, because usually the interfacial tensions  $\sigma_B^F$  and  $\sigma_D^F$  cannot be measured separately. Instead, the film tension  $\gamma$  is calculated from the experimentally measured contact angle  $\theta$  (see Figure 12). The relationship between  $\gamma$  and  $\theta$  for a given system is derived by performing a force balance at the film perimeter.<sup>1,2</sup> For the nonsymmetric system considered here and in the absence of line tension effects we have:

$$\gamma^2 = (\sigma_D + \sigma_B)^2 - 2\sigma_B\sigma_D(1 - \cos \theta) \quad (\text{A7})$$

Since with the approximation adopted here  $\gamma \approx \sigma_B^F + \sigma_D^F$  (see eq A4 with  $x = x_B = x_D = 0$ ), the sum of the interfacial tensions is also measurable and its change

$$\Delta\sigma = (\sigma_D^F + \sigma_B^F) - (\sigma_D + \sigma_B) \quad (\text{A8})$$

(due to the interaction between the surfaces, i.e., to the disjoining pressure) can be determined experimentally.

Exact expressions for the relationship between the film interfacial tensions and the disjoining pressure are given by eq 136 in ref 36. In the framework of the linear

approximation in terms of  $x$  they read (at constant temperature and chemical potentials):

$$d\sigma_D^F = -\Pi(1 + 2x_D)dh_D; \quad d\sigma_B^F = -\Pi(1 - 2x_B)dh_B \quad (\text{A9})$$

Neglecting again the  $x$ -terms and summing up the results leads to  $d(\sigma_B^F + \sigma_D^F) = -\Pi dh$ , which upon integration from  $h$  to infinity (where the disjoining pressure is zero) yields the correction  $\Delta\sigma$  sought for (see eq A8 above):

$$\Delta\sigma = \int_h^\infty \Pi(h)dh \quad (\text{A10})$$

The coincidence of the expressions for  $d\Pi$  for the two interfaces (with the respective  $x$ 's equal to zero) suggests that the corrections of the respective interfacial tensions are both equal to  $\Delta\sigma/2$  (although  $\sigma_D^F$  and  $\sigma_B^F$  themselves are not equal).<sup>40</sup> Then substituting in eq A6  $\sigma_D^F = \sigma_D + \Delta\sigma/2$  and  $\sigma_B^F = \sigma_B + \Delta\sigma/2$ , and keeping only the linear terms with respect to  $\Delta\sigma/\sigma$ , after simple calculations we obtain the final expression for  $\Pi$  in terms only of measurable quantities (interfacial tensions, capillary pressures and  $\Delta\sigma$ ):

$$\Pi = \frac{\sigma_D P_C^B + \sigma_B P_C^D}{\sigma_B + \sigma_D} \left( 1 - \frac{\Delta\sigma}{\sigma_B + \sigma_D} \right) + \frac{\Delta\sigma}{2(\sigma_B + \sigma_D)} (P_C^B + P_C^D) \quad (\text{A11})$$

In conclusion we will notice that the term  $\Pi R_{fx}$  in eq A4 is not related to the film curvature. Indeed, it stems from the finite film thickness and is present and equal also to  $\Pi h$  for planar films (see, e.g., ref 36 and eq A5). Hence, for very small drops, when  $x$  may become comparable to  $\Delta\sigma/\sigma$ , more detailed analysis is needed, when establishing the connection between  $\gamma$  and  $\sigma_B^F + \sigma_D^F$ .

LA010751U

(40) By making in eq A9 the very reasonable approximation  $h_B = h_D = h/2$ , one can show that this conclusion is true even when the linear terms in  $x$  are kept.